Elastic tunneling charge transport mechanisms in silicon quantum dots /SiO_2 thin films and superlattices

S. Illera,[a] J. D. Prades, and A. Cirera
MIND/IN2UB Departament d'Electrònica, Universitat de Barcelona, C/Martí i Franquès 1, E-08028 Barcelona, Spain

(Received 22 December 2014; accepted 23 April 2015; published online 4 May 2015)

The role of different charge transport mechanisms in Si/SiO_2 structures has been studied. A theoretical model based on the Transfer Hamiltonian Formalism has been developed to explain experimental current trends in terms of three different elastic tunneling processes: (1) trap assisted tunneling; (2) transport through an intermediate quantum dot; and (3) direct tunneling between leads. In general, at low fields carrier transport is dominated by the quantum dots whereas, for moderate and high fields, transport through deep traps inherent to the SiO_2 is the most relevant process. Besides, current trends in Si/SiO_2 superlattice structure have been properly reproduced.
 [http://dx.doi.org/10.1063/1.4919747]

I. INTRODUCTION

Silicon quantum dots (Si Qd) embedded in insulator matrices have opened a new branch of devices in electronics and photonics: single-electron transistors,[1] new memory concepts,[2] and photon or electroluminescent devices.[3]

An experimental route, the superlattice approach (SL),[4] was developed to create these Si Qds embedded in SiO_2 matrices, where thin silicon rich oxide (SRO) and thin SiO_2 layers are deposited alternatively. In a later temperature annealing process, Qds are formed in the SRO layer and these SiO_2 layers remain as diffusion barriers. The Qd size, and their energy gap,[5] can be controlled tuning the width of the layer. These structures have been proposed to build light absorbers for third generation photovoltaic applications.[6–8] However, the large band offsets between Si and SiO_2 ($\approx$3.1 eV and $\approx$4.5 eV for conduction and valence band, respectively) focus the problem on the charge transport through the oxide matrix.

Due to the absence of a complete theoretical framework that describes in full the complex electrical response of this kind of systems, three basic expressions are usually used to fit different regimes of the experimental current measurements. Poole-Frenkel (P-F)[9–11] fit is often used where the current-field dependence $J(F)$ is $J \propto F \cdot \exp(a\sqrt{F/\epsilon_r})$, being ϵ_r the relative permittivity. The trap-assisted tunneling (TAT)[12] model predicts $J \propto \exp(a \cdot \phi_t^{3/2}/F)$, where ϕ_t is the mean trap energy, and the Fowler-Nordheim tunneling (FN)[13] model establishes $J \propto F^2 \cdot \exp(a \cdot \phi_b^{3/2}/F)$, where ϕ_b is the barrier height. However, these expressions usually only fit in small electric field ranges of the experimental data, and the fitted parameters usually disagree with the experimental ones,[14] lacking of a real physical meaning. Moreover, several experimental charge transport and charge trapping studies in superlattice structures have also been carried out[15,16] showing that the underlying transport mechanism cannot be ascribed to any of these well-known expressions for charge transport in dielectrics. As this kind of structures will conform the core of the new optoelectronic devices based on Qds, knowledge of the underlying physics and a correct description of the electronic transport are still necessary.

From a theoretical point of view, the electronic transport through a single Qd has been widely studied by many authors and novel transport phenomena have been discovered such as: the staircaselike current-voltage characteristic,[17] Coulomb blockade oscillation,[18] negative differential capacitance,[19] and the Kondo effect.[20] Although many authors have described the electron transport using Non-Equilibrium Green Functions Formalism (NEGFF),[21,22] this approach is unsuitable for large systems such as the ones studied here. In contrast, the Transfer Hamiltonian Formalism (THF)[23,24] has been successfully used previously in combination with a rate equation model to describe large Qds arrays obtaining similar results than NEGFF.[25] Moreover, the THF has been also used to describe the trap assisted tunneling in different degrees of sophistication.[26–28] However, up to now, nobody has presented a complete transport model capable to simulate large Qd arrays and traps (or defects) associate to the Qd formation or intrinsic to the dielectric matrix. In summary, theoretical models and experimental systems are still far from each other.

In this work, we provide an explanation to the charge transport features observed experimentally in Si/SiO_2 thin films and superlattice structures based on elastic tunneling mechanisms described within the THF. Three kinds of ballistic charge transport mechanism are considered, reproducing the experimental trends in Si/SiO_2 configurations.

II. THEORETICAL MODELS

The possible elastic tunneling transport processes in SiO_2 based structures are shown in Fig. 1: through the total oxide for low and high fields (process I and II), assisted by an intermediate trap (process III), and assisted by a Qd (process IV).

[a]sillera@el.ub.edu

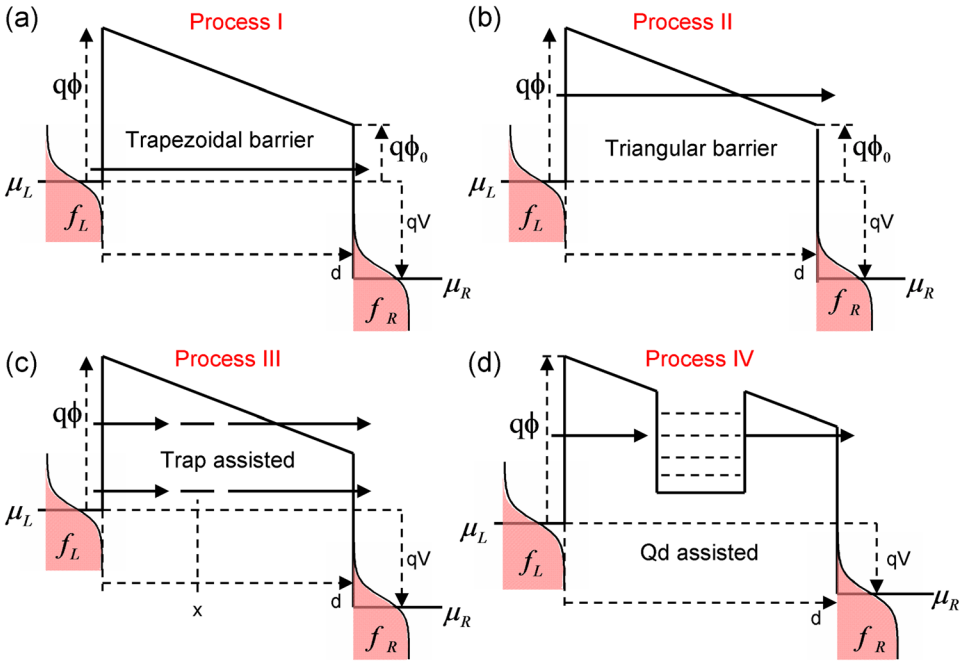

FIG. 1. Energy band diagram of the system under external electric field. The different elastic tunneling transport processes are also shown: (a) tunneling from left to right lead through a trapezoidal potential barrier (process I) and (b) through a triangular one (process II). (c) Assisted tunneling via an intermediate trap (process III) and (d) assisted by a Qd (process IV). The Fermi level of each lead (μ_L and μ_R) and the Fermi function (f_L and f_R) are also shown. μ_L is fixed as the energy reference.

The expression for the current associated to the tunneling mechanisms I and II can be written using the THF as[23,24]

$$I_{FN} = \frac{4\pi^2 q}{h}\int_{-\infty}^{+\infty} T(E)\rho_R(E)\rho_L(E)\big(f_L(E) - f_R(E)\big)dE, \quad (1)$$

where $\rho_L(E)$ and $\rho_R(E)$ are the densities of states (DOSs) of the left and right lead, respectively. The occupation distribution functions of the leads are well described by the Fermi functions, $f_L(E)$ and $f_R(E)$, with the corresponding electrochemical potential for the left and right leads, μ_L and μ_R, respectively. Under an external bias voltage V_{gate}, we can write $\mu_L - \mu_R = qV_{gate}$. We choose the Wentzel-Kramers-Brillouin (WKB) approximation[29] to describe the tunneling probability $T(E)$ for an electron to cross the oxide barrier from one side to the other side via an elastic tunnel process (ballistic transport). From the WKB approximation, taking into account the band bending of the oxide bands due to the external applied voltage and assuming that the voltage drops uniformly in all the insulator, the value of the potential barrier along the tunneling direction reads as $q\phi(x) = q\phi - qE_{diel}x$. Using the WKB approximation and the position dependent potential barrier, we can write the transmission coefficient as

$$T = \begin{cases} \exp\left\{-4\dfrac{\sqrt{2m^*_{diel}}}{3\hbar qF}\left((q\phi - E)^{3/2} - (q\phi_0 - E)^{3/2}\right)\right\} \text{ for } \quad q\phi_0 \geq E \\ \exp\left\{-4\dfrac{\sqrt{2m^*_{diel}}}{3\hbar qF}(q\phi - E)^{3/2}\right\} \text{ for } \quad q\phi \geq E \geq q\phi_0, \end{cases} \quad (2)$$

where $q\phi$ is the potential barrier height, the electric field is defined as $F = \frac{\mu_L - \mu_R}{qd}$ (assuming that the voltage drops uniformly along the insulator), and d is the total oxide thickness. The modified potential barrier ($q\phi_0$) is defined as $q\phi(d)$, where d is the tunneling distance and m^*_{diel} is the electron oxide effective mass. The term $\frac{\mu_L - \mu_R}{q}$ reflects the different bias voltage applied to each side of the barrier. We used the simplest expression for elastic tunneling probability assuming uniform field in the dielectric matrix and neglecting image force effects, since the WKB approximation reproduces the exact solution for the thickest barriers. However, the exact solution of the transmission coefficient for trapezoidal and triangular barriers can be obtained using the transfer matrix approach,[30] or expressed in terms of Airy's functions.[13,31]

There is some controversy about the inclusion of the image force effects in the calculation of the tunnel current. Some authors argue that its inclusion overestimates the tunneling current,[32,33] and other authors claim for its inclusion in order to avoid the thickness-dependent tunneling mass.[34,35] In any case, the inclusion of the image force is known to lower and round the barrier edge, which can be included just changing the barrier height. Thus, we can avoid the image force, specially if the barrier height is used as a fitting parameter. Complete studies about the inclusion of image effects and how they affect the potential barrier can be found elsewhere.[36–38]

Remarkably, two main transmission expressions appear, as a function of the energy of the incident electrons and the

band bending of the insulator. The first expression has been widely used by several research groups[39–41] to interpret their experimental current measurements as tunneling through a trapezoidal barrier (process I). The second transmission expression reflects the tunneling through a triangular barrier (process II),[42,43] and it is usually used for high fields.

Elastic trap-assisted tunneling (process III) is described as a two-step process. Electrons come from one lead to the trap and then go out to the second lead. Writing the occupation of a single mono-energetic trap as a net flux between incoming and outgoing current, and assuming a steady state condition, the net current that crosses the oxide through the trap from lead to lead can be written as[44]

$$I(E_t, V_{gate}) = 2\frac{q^2}{\hbar}\frac{T_L(E_t)T_R(E_t)}{T_L(E_t)+T_R(E_t)}(f_L(E_t)-f_R(E_t)), \quad (3)$$

where we used the THF to describe the partial fluxes. The occupation functions of the leads are described by the Fermi function, $f_L(E_t)$ and $f_R(E_t)$, with the corresponding electrochemical potential for the left and right leads, respectively. $T_L(E_t)$ and $T_R(E_t)$ are the tunneling probabilities for the left and right contacts and they are described using Eq. (2). The expression presented in Eq. (3) is a particular case for a single energy level of the most general expression for current in the ballistic transport regime derived in detail in Ref. 44. We must note here that all these parameters are evaluated at the energy level of the trap E_t, since we consider that the trap is mono-energetic. The unbiased trap energy level E_0 is usually measured from the bottom of the conduction band but for convenience, we redefine the energy origin to the position of the equilibrium Fermi level.

On the other hand, the energy level of the trap is located at a constant energy position from the bottom of the oxide conduction band. We assume that when an external voltage V_{gate} is applied, the voltage drops uniformly through the oxide, bending the conduction band and modifying the energy level position of the trap. The position of the trap energy level is described by $E_t(x, V_{gate}) = E_0 - \frac{qV_{gate}}{d}x$, where x is the distance respect to the left lead and d is the total oxide thickness.

In Eq. (3), the current expression through a single trap was presented, but we can use it to simulate the total current for a trap distribution in energy, $f_t(E_0, x)$. The total trap current reads as

$$I_{Traps}(V_{gate}) = \int_0^d \int_{E_{0min}}^{E_{0max}} f_t(E_0, x) I(E_t, V_{gate}) dx\, dE_0, \quad (4)$$

where E_{0min} and E_{0max} are the minimum and maximum energy distance between the traps and the bottom of the oxide conduction band, respectively. From Eq. (4) and the single trap current expression Eq. (3), the two main parameters that govern the final current value, for an externally applied bias voltage, are: (1) the trap position (x) and (2) the energy level distribution (E_0).

Concerning the elastic transport through an intermediate Qd embedded in the oxide matrix (process IV), we use the formalism developed in Ref. 45. It describes the carrier transport through a system of Qds, using rate equations to obtain the non-equilibrium distribution functions of each Qd and the trapped charge. Discrete DOSs are obtained describing the Qds as isolated finite spherical potential wells. The effect of the external polarization is included via capacitive couplings. Furthermore, the system is evaluated in the self consistent field regime (SCF) taking into account the repulsion effect of the charge accumulated in each Qd. That methodology was compared with NEGFF obtaining similar results but using a simpler and more intuitive theoretical approach.[25] A detailed explanation of the methodology can be found in Ref. 46 and its application to realistic Qds described with *ab initio* techniques is presented in Ref. 47.

From the three previously described current terms, and assuming that the leads act as infinite carrier reservoirs, the total current, I_{total}, can be expressed as

$$I_{total} = I_{FN} + I_{Traps} + I_{Qd}. \quad (5)$$

We must note here that we neglected the interaction between the Qds and the traps, since we considered both processes as independent transport channels. This assumption, that seems dramatic, can be justified thinking in terms of the tunnel current values. The tunnel current depends on the DOS at both sides of the barrier. Therefore, the current between a Qd and a single trap is lower than the current between Qds. Thus, the first one can be neglected. For the same reason, the current between traps is not considered (i.e., the transport processes that involves two or more intermediate traps).

III. TRANSPORT SIMULATIONS

The previous model was used to reproduce the electrical measurements of three different Si/SiO_2 structures, which are basically MOS-like structures: as P-type Si substrate and a highly N-type doped polycrystalline silicon (polysilicon) were, respectively, used as rear and top electrodes. The different active layers embedded between both electrodes are: (1) a SiO_2 layer of different thicknesses (SiO_2); (2) Si Qds randomly distributed in a SiO_2 matrix (Si Qd/SiO_2); and (3) a superlattice structure of 6 SRO/SiO_2 bilayers (SL Si Qd/SiO_2).

The expressions for the current previously presented (Eqs. (1), (3), and (4)) are basically well described by the electron effective mass in the oxide $m_{diel} = 0.3m_0$ (Ref. 48) (where m_0 is the free electron mass) and the Si/SiO_2 electron potential barrier height $q\phi = 3.1\,\text{eV}$.[48] All the parameters needed to describe the Si Qds array embedded in SiO_2 were extracted from Ref. 46. All the simulations were carried out at room temperature ($k_BT = 0.026\,\text{eV}$). In order to reflect the intrinsic properties of the different active layers under study, we assumed a continuous and uniform lead DOS (ρ_L and ρ_R).

First of all, we studied the tunnel transport processes through a pure SiO_2 film with different thicknesses in order to validate the here presented trap assisted model. Fig. 2(a) shows the simulated and the experimental tunnel current density through SiO_2 for different thicknesses. Experimental current density measurements were taken from Ref. 49. We used the SiO_2 parameters to explain the tunneling processes (the values used are described in Appendix A). A Gaussian distribution function in energy was assumed to describe the mono-energetic trap distribution, following:

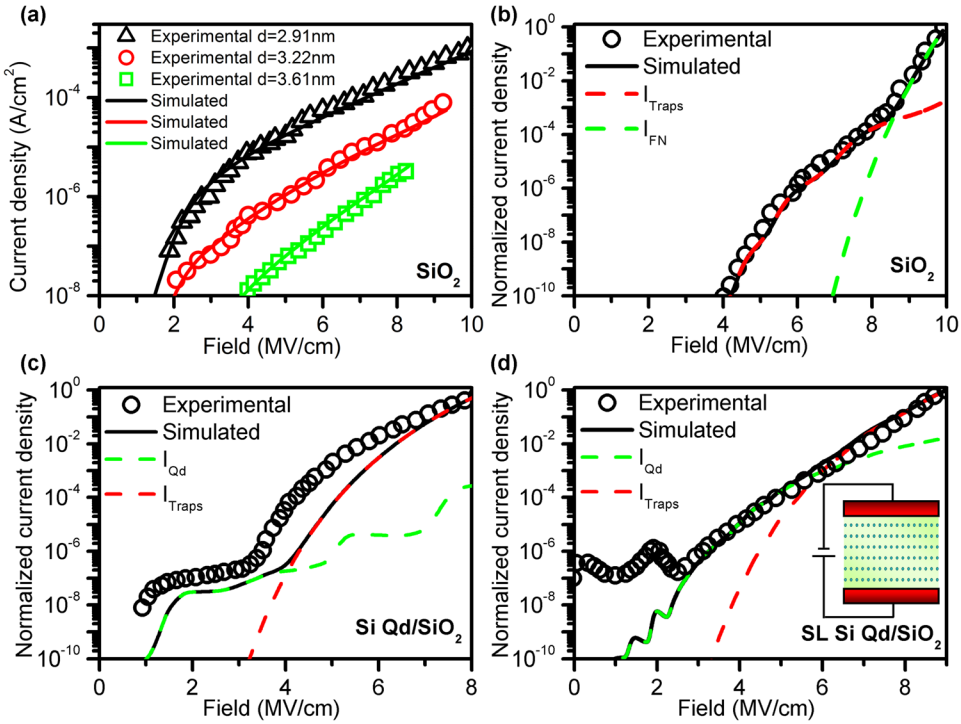

FIG. 2. (a) Experimental and simulated tunnel current densities for different SiO_2 active layer thicknesses. Experimental data have been extracted from Ref. 49. (b) Normalized current density (experimental and simulated) for the SiO_2 structure. Trap (I_{Traps}) and direct tunnel (I_{FN}) currents are also shown. (c) Normalized current density (experimental and simulated) for the Si Qd/SiO_2 structure. Current through the Qds (I_{Qd}) and the traps (I_{Traps}) is shown. (d) Normalized current density (experimental and simulated) for the SL Si Qd/SiO_2 structure. Different current contributions and the cross section of the superlattice structure are also shown. The experimental data of (b)–(d) have been extracted from Ref. 50.

$$f_t(E_0,x)=\begin{cases} N_0\cdot\exp\left\{-\left(\dfrac{E_0-\langle E_0\rangle}{\sigma_{E_0}}\right)^2\right\} & \text{for} \quad E_0\in[E_{0min},E_{0max}] \\ 0 \quad \text{for} \quad E_0\notin[E_{0min},E_{0max}], \end{cases} \tag{6}$$

where N_0 is the trap density, $\langle E_0\rangle$ is the average of the distribution, and the width is controlled by σ_{E_0}. The traps were distributed uniformly in space being the energy distribution independent of the trap position. The best fit parameters are presented in Table I. Besides, we compared our fits and the resulting parameters fitted with the approach presented on Ref. 28. The authors of Ref. 28 presented a complete theoretical model based on the THF to study the trap-assisted elastic tunneling and analyzed the role of the image force. Detailed expressions for the tunneling probabilities were also presented. In order to make a direct comparison between both approaches, we used their fitted active layer thicknesses: 2.91 nm, 3.22 nm, and 3.61 nm.

As we can see in Fig. 2(a), our elastic tunneling trap assisted model successfully reproduces the experimental results. The parameters used to describe the position and energy trap distribution functions are similar to the ones used in Ref. 28. We focused on the thickest active layers since, as Ref. 28 claimed, for the thinner ones the experimental data were well reproduced taking into account only the tunneling from one lead to the other without intermediate tunneling processes. In the thickest samples, the tunnel current through the total oxide (process I and II) slightly underestimates the experimental current, and the inclusion of elastic tunneling assisted by traps is needed to reproduce the experimental trends. Small discrepancies arise in the fitted parameters, since the authors of Ref. 28 considered an energy dependent oxide effective mass whereas we used the previous constant value. However, both models describe the elastic trap-assisted tunneling using similar trap densities and energy distribution function. From this comparison, in the next simulations, we consider a fixed value of $\langle E_0\rangle = 1.3$ eV and $\sigma_{E_0} = 0.45$ eV for the energy trap distribution. For further information, in Appendix B, we studied the changes predicted by Eq. (3) as a function of the trap energy level and its position.

TABLE I. Parameters of the trap distribution used to fit the experimental data and its comparison to other theoretical approach. We have used $E_{0min} = 0.3$ eV and $E_{0max} = 3$ eV for all the fits.

d (nm)	N_0 (cm^{-3})	$\langle E_0\rangle$ (eV)	σ_{E_0} (eV)	
2.91 nm	6.87×10^{13}	1.25	0.48	This work
	4×10^{14}	1.0	0.65	Ref. 28
3.22 nm	1.24×10^{13}	1.25	0.48	This work
	1×10^{14}	0.8	0.65	Ref. 28
3.61 nm	5.54×10^{12}	1.40	0.39	This work
	3×10^{13}	1.1	0.65	Ref. 28

Reference 50 reports on the current density through different Si/SiO_2 structures: a 50 nm thick SiO_2 active layer, a 50 nm SRO single layer (Si Qd/SiO_2), and a superlattice structure of 6 SRO/SiO_2 bilayers (SL Si Qd/SiO_2). In the last two structures, they showed Qds embedded in the dielectric matrix.

Concerning the SiO_2 layer, the simulated current and the experimental data are shown in Fig. 2(b). For low and

moderate fields, the elastic trap assisted tunneling mechanism dominates transport, and for high fields the oxide band bending allows direct tunnel from the left to the right lead. It is worth to mention that the trap energy level considered in our simulations correlates well with the one fitted by the authors (1.2 eV).[50] In Appendix C, we present the charge trapped distribution in the oxide as a function of the electric field.

Regarding the Si Qd/SiO_2 structure, it is basically a SiO_2 layer in which the silicon excess aggregates forming Si Qds. We used here the Qd transport model in combination with the elastic trap assisted tunneling. The simulated current and the experimental data are shown in Fig. 2(c). According to microscopic measurements from Ref. 50, we simulated an arrangement of Qds in random positions and normal radius distribution with $\langle R \rangle = 1.5$ nm of mean radius and $\sigma_R = 0.2$ nm of standard deviation. We used the same monoenergetic trap distribution as in the previous case. Fig. 2(c) also shows the different current contributions due to the transport: through the Qds and through the traps. We distinguish two main regimes: the Qd term displays the step-like behavior in the current as a consequence of the discrete nature of the Qd energy levels and it is the dominant transport mechanism for low fields, whereas for intermediate and high fields the trap assisted tunneling dominates. We must note that these results can not be achieved considering direct tunnel between the leads, so we concluded that the electron transport process is assisted by an intermediate Qd or a trap. In this case, the authors of Ref. 50 fit a TAT expression with a mean energy trap value (1.8 eV) for moderate and high fields. The fitted value is different to the one used in the SiO_2 structure, and they claim that the transport is assisted by Si Qds and SiO_2 traps. However, a further explanation is needed for the obtained current behavior at low fields. Our simulations reproduce the experimental behavior and give an explanation for the low field regime, as pure transport through the discrete energy states of the Qds. When an energy state of the Qd lies between the electrochemical potential of the leads, a conduction channel is opened and the current increases in discrete steps. Besides, traps also contribute to the total current being the dominant process for moderate and high fields. However, some discrepancies appear for higher voltages. We note here that we used the previous trap energy distribution neglecting the possibility that the Qds change the energy levels of the traps.

Finally, the simulated current and the experimental results for the SL Si Qd/SiO_2 are shown in Fig. 2(d). An scheme of the structure is also presented in the inset of Fig. 2(d). In order to properly describe the structure presented in Ref. 50, we considered 6 layers of Si Qds with a normal distribution of radius, $\langle R \rangle = 1.5$ nm of mean radius and $\sigma_R = 0.2$ nm of standard deviation. The Qds were distributed in a perpendicular plane respect to the transport direction reflecting the layered structure (each two layers were spaced 2.5 nm). As in the previous case, we used the Qd transport model and the trap assisted tunneling. The total current was decomposed in these two terms. For low field regime, we reproduced the current peaks and their explanation is related to the different Qds capacitive couplings and the DOS overlapping between the Qds, which open and close the conductive channels.[25] For the highest fields, a pure trap mechanism is enough to explain the experiments results. In Ref. 50, the authors fitted a P-F expression for moderate fields, and a pure TAT for higher fields with a mean energy trap value (1 eV), neglecting the current peaks at low fields. This value is close to the one obtained for the SiO_2 structure, and the authors concluded that the tunneling in both structures is mediated by deep traps inherent to the SiO_2 and not by states created *ad-hoc* when including Si Qds. This fact is directly reflected here, since we considered a fixed value for the energy level trap distribution.

IV. CONCLUSIONS

A charge transport model based on the Transfer Hamiltonian Formalism has been presented to describe the different ballistic transport mechanisms. The model has been used to reproduce experiments from different Si/SiO_2 structures, and it is only based on a reduced set of physically meaningful constants. Simulations allowed us to explain the transport in these structures as follows: (i) for pure SiO_2 layers, trap assisted tunneling dominates at low and moderate fields whereas for high fields direct tunnel between leads is the most important process; (ii) in the presence of Si Qds, the current reflects the discrete nature of the energy levels for low electric fields and trap assisted tunneling appears for moderate and high fields. All this demonstrates that the method can be extended to extract empirical parameters from complex current/field curves in nanodevices.

ACKNOWLEDGMENTS

S. Illera was supported by the FI programme of the Generalitat de Catalunya. J. D. Prades acknowledges support from the Serra Húnter Programme. A. Cirera acknowledges support from ICREA academia program. The authors thank to Dr. Y. Berencen for all the valuable comments about the manuscript and enlightening discussions. The research leading to these results has received funding from the European Community's Seventh Framework Programme (FP7/2007-2013) under Grant Agreement No. 245977.

APPENDIX A: MATERIAL AND SYSTEM PARAMETERS

Here, we summarize the material and geometrical parameters used in the simulations. The transmission coefficients are well described by the oxide effective mass $m_{diel} = 0.3m_0$, where m_0 is the free electron mass, and the Si/SiO_2 potential barrier $q\phi = 3.1$ eV. For Figs. 2(b)–2(d), we assumed $\langle E_0 \rangle = 1.3$ eV, $\sigma_{E_0} = 0.45$ eV, and a uniform space distribution for the traps.

The simulations were done at $k_BT = 0.026$ eV and the values of $\rho_{L/R}(E)$ were assumed as energy constants. Concerning the Si Qd transport model and the used parameters, they are presented in detail in Ref. 46.

The geometry of the systems simulated in Figs. 2(b)–2(d) is summarized in Table II.

TABLE II. Geometrical active layer parameters for the systems presented in Figs. 2(b)–2(d), respectively.

SiO_2	$d = 50\,\text{nm}$
Si Qd/SiO_2	$d = 50\,\text{nm}$
	$\langle R\rangle = 1.5\,\text{nm}$
	$\sigma_R = 0.2\,\text{nm}$
SL Si Qd/SiO_2	$d = 50\,\text{nm}$
	$\langle R\rangle = 1.5\,\text{nm}$
	$\sigma_R = 1.5\,\text{nm}$
	$d_{layer} = 2.5\,\text{nm}$

The thickness of the active layer is d, the Qds were generated assuming a normal distribution in radius assuming $\langle R\rangle$ for mean value and σ_R as standard deviation. In the bilayer structure, the distances between Qds layers were d_{layer}.

APPENDIX B: CURRENT THROUGH A SINGLE TRAP

As it can be inferred from Eq. (3) and from the tunneling probabilities, Eq. (2), the current through a single trap is strongly dependent on its position and the trap energy level. Here, we present current maps, Fig. 3, as a function of the trap distance to the left lead (x) and the mono-energetic trap level (E_0) for the thickest SiO_2 layer ($d = 3.61\,\text{nm}$) under different electric fields.

Generally speaking, in order to obtain ballistic transport through a energy level E_t, this level has to lie between the electrochemical potentials of the leads (μ_L and μ_R). This condition is written in Eq. (3) as the difference of the Fermi functions evaluated at this energy, $f_L(E_t) - f_R(E_t)$. The evolution of the trap energy level as a function of the electric field includes the position dependence of the trap. Moreover, the tunneling distance and field dependencies are included in the transmission coefficients.

In Fig. 3, the dominant trap current is shown for different applied electric fields. When the field increases, the band bending of the oxide increases and the traps which are located closer to the left lead with the highest energy levels are the most conductive ones, since they see lower potential barriers.

APPENDIX C: TAP CHARGE DISTRIBUTION

Here, we present the trapped charge distribution in space for different fields, as a function of the applied electric field for the 50 nm SiO_2 active layer. The results are shown in Figs. 4(a) and 4(b), respectively.

The charge injection in the oxide is a balance between the incoming and the outgoing carrier fluxes to/from the leads, and it is strongly dominated by the tunneling probability that depends on the position of the trap and the applied electric field. Following the derivation of Ref. 44, the charge in a mono-energetic trap can be written as

$$N = \frac{T_L(E_t)f_L(E_t) + T_R(E_t)f_R(E_t)}{T_L(E_t) + T_R(E_t)}. \tag{C1}$$

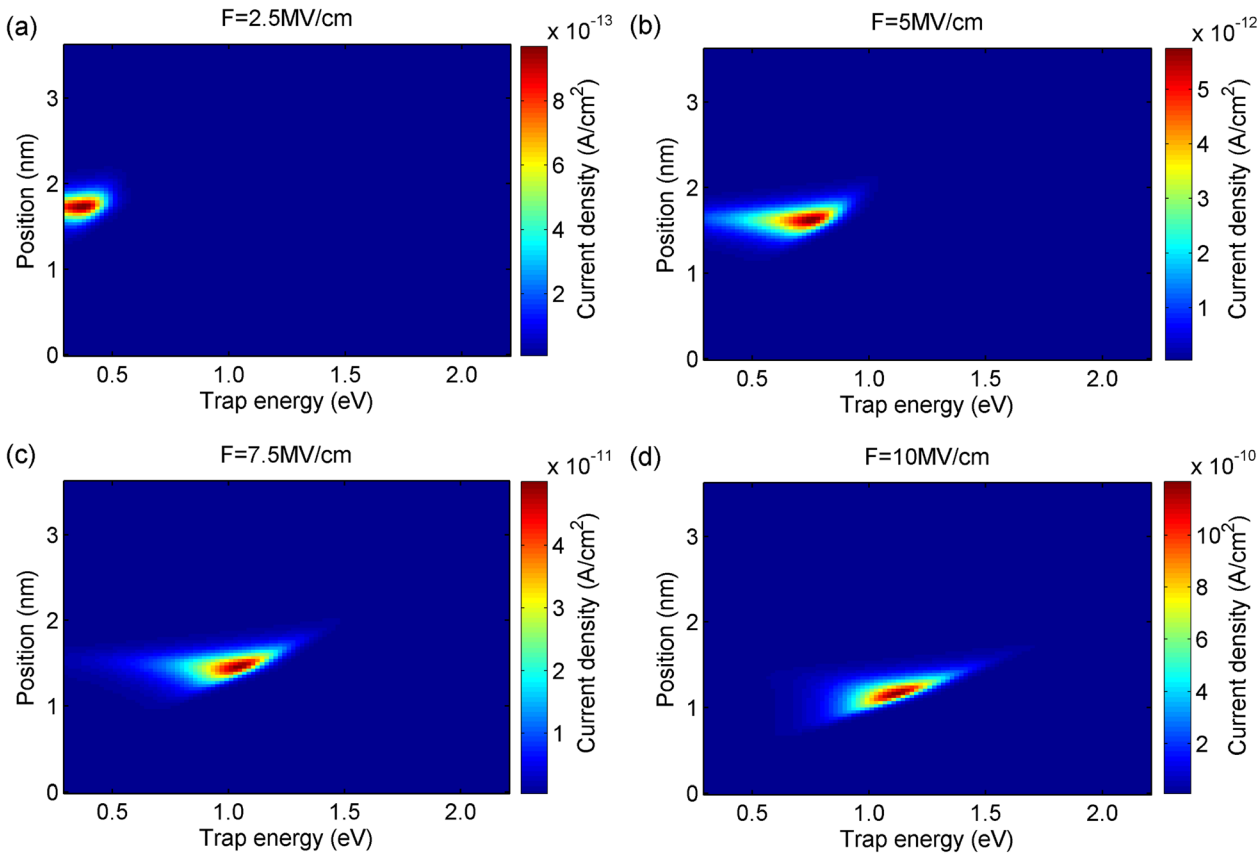

FIG. 3. Current map for a single trap as a function of the distance to the left lead and the energy trap level for different electric fields: (a) $F = 2.5\,\text{MV/cm}$, (b) $F = 5\,\text{MV/cm}$, (c) $F = 7.5\,\text{MV/cm}$, and (d) $F = 10\,\text{MV/cm}$.

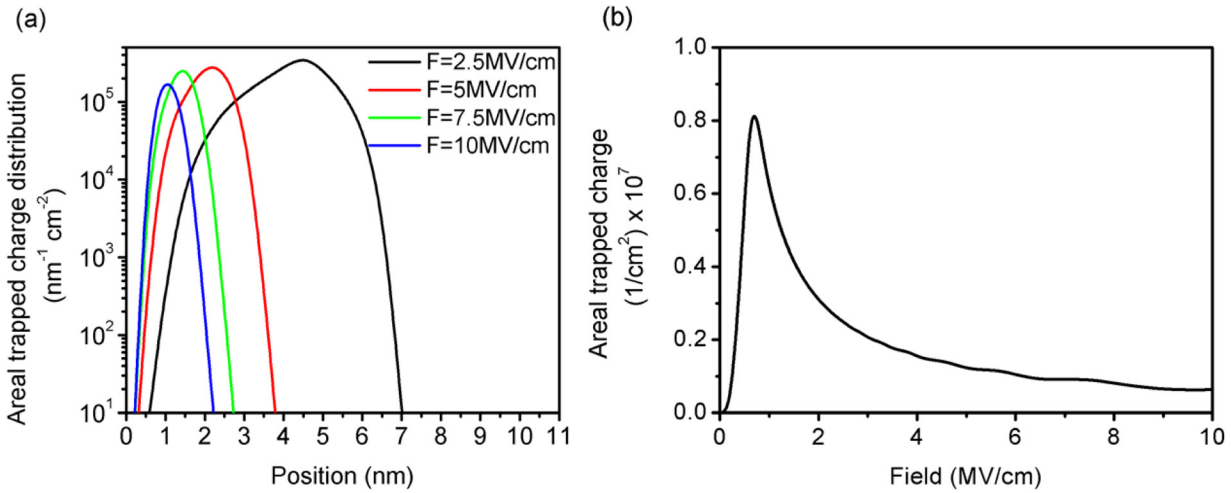

FIG. 4. Trapped charge studies for the 50 nm SiO_2 layer. (a) Trapped charge distribution in the oxide layer for different electric fields and (b) trapped charge as a function of the applied electric field.

In Fig. 4(a), we show the trapped charge distribution in the oxide layer for different electric fields. When the field increases, all the charge is concentrated in the interface between the left lead and the oxide layer being possible to create internal electric field that reduces the contact potential barrier (image charge effects). However, further explanation is necessary since in Fig. 2(b) the simulated curves matched the experimental trends, whereas in Fig. 2(c) the trend is not recovered reflecting that the Qds play an important role.

The trapped charge as a function of the applied electric field is shown in Fig. 4(b) obtaining a maximum trapped charge when $T_L(E_t) > T_R(E_t)$ and E_t lies between μ_L and μ_R ($f_L(E_t) \approx 1$ and $f_R(E_R) \approx 0$).

[1]U. Meirav and E. B. Foxman, Semicond. Sci Technol. **11**, 255 (1996).
[2]S. Tiwari, F. Rana, K. Chan, L. Shi, and H. Hanafi, Appl. Phys. Lett. **69**, 1232 (1996).
[3]D. J. Lockwood, *Semiconductor and Semimetals, Light Emission in Silicon from Physics to Devices* (Academic Press, San Diego, 1998).
[4]M. Zacharias, J. Heitmann, R. Scholz, U. Kahler, M. Schmidt, and J. Blsing, Appl. Phys. Lett. **80**, 661 (2002).
[5]J. P. Proot, C. Delerue, and G. Allan, Appl. Phys. Lett. **61**, 1948 (1992).
[6]T. Kirchartz, K. Seino, J.-M. Wagner, U. Rau, and F. Bechstedt, J. Appl. Phys. **105**, 104511 (2009).
[7]G. Conibeer, M. Green, R. Corkish, Y. Cho, E.-C. Cho, C.-W. Jiang, T. Fangsuwannarak, E. Pink, Y. Huang, T. Puzzer, T. Trupke, B. Richards, A. Shalav, and K. L. Lin, Thin Solid Films **511–512**, 654 (2006).
[8]E.-C. Cho, S. Park, X. Hao, D. Song, G. Conibeer, S.-C. Park, and M. A. Green, Nanotechnology **19**, 245201 (2008).
[9]T. Creazzo, B. Redding, E. Marchena, J. Murakowski, and D. W. Prather, J. Lumin. **130**, 631 (2010).
[10]A. Irrera, F. Iacona, I. Crupi, C. D. Presti, G. Franz, C. Bongiorno, D. Sanfilippo, G. D. Stefano, A. Piana, P. G. Fallica, A. Canino, and F. Priolo, Nanotechnology **17**, 1428 (2006).
[11]S. Prezioso, A. Anopchenko, Z. Gaburro, L. Pavesi, G. Pucker, L. Vanzetti, and P. Bellutti, J. Appl. Phys. **104**, 063103 (2008).
[12]W.-J. Chang, M.-P. Houng, and Y.-H. Wang, J. Appl. Phys. **90**, 5171 (2001).
[13]R. H. Fowler and L. Nordheim, Proc. R. Soc. London, Ser. A **119**, 173 (1928).
[14]M. A. Rafiq, Z. A. K. Durrani, H. Mizuta, M. M. Hassan, and S. Oda, J. Appl. Phys. **104**, 123710 (2008).
[15]S. Gutsch, J. Laube, A. M. Hartel, D. Hiller, N. Zakharov, P. Werner, and M. Zacharias, J. Appl. Phys. **113**, 133703 (2013).
[16]J. López-Vidrier, Y. Berencén, S. Hernández, O. Blázquez, S. Gutsch, J. Laube, D. Hiller, P. Loper, M. Schnabel, S. Janz, M. Zacharias, and B. Garrido, J. Appl. Phys. **114**, 163701 (2013).
[17]J. B. Barner and S. T. Ruggiero, Phys. Rev. Lett. **59**, 807 (1987).
[18]J. Weis, R. J. Haug, K. V. Klitzing, and K. Ploog, Phys. Rev. Lett. **71**, 4019 (1993).
[19]S. D. Wang, Z. Z. Sun, N. Cue, H. Q. Xu, and X. R. Wang, Phys. Rev. B **65**, 125307 (2002).
[20]W. G. van der Wiel, S. D. Franceschi, T. Fujisawa, J. M. Elzerman, S. Tarucha, and L. P. Kouwenhoven, Science **289**, 2105 (2000).
[21]A. L. Yeyati, A. Martin-Rodero, and F. Flores, Phys. Rev. Lett. **71**, 2991 (1993).
[22]Y. Meir and N. S. Wingreen, Phys. Rev. Lett. **68**, 2512 (1992).
[23]M. C. Payne, J. Phys. C: Solid State Phys. **19**, 1145 (1986).
[24]M. Passoni and C. E. Bottani, Phys. Rev. B **76**, 115404 (2007).
[25]S. Illera, N. Garcia-Castello, J. D. Prades, and A. Cirera, J. Appl. Phys. **112**, 093701 (2012).
[26] Khairurrijal, W. Mizubayashi, S. Miyazaki, and M. Hirose, J. Appl. Phys. **87**, 3000 (2000).
[27]O. Blank, H. Reisinger, R. Stengl, M. Gutsche, F. Wiest, V. Capodieci, J. Schulze, and I. Eisele, J. Appl. Phys. **97**, 044107 (2005).
[28]F. Jiménez-Molinos, F. Gámiz, A. Palma, P. Cartujo, and J. A. López-Villanueva, J. Appl. Phys. **91**, 5116 (2002).
[29]J. J. Sakurai, *Modern Quantum Mechanics* (Addison Wesley, 1994), p. 104.
[30]S. Vatannia and G. Gildenblat, IEEE J. Quantum Electron. **32**, 1093 (1996).
[31]K. Gundlach, Solid-State Electron. **9**, 949 (1966).
[32]Z. Weinberg and A. Hartstein, Solid State Commun. **20**, 179 (1976).
[33]A. Hartstein and Z. A. Weinberg, J. Phys. C: Solid State Phys. **11**, L469 (1978).
[34]G. Binnig, N. Garcia, H. Rohrer, J. M. Soler, and F. Flores, Phys. Rev. B **30**, 4816 (1984).
[35]A. Schenk and G. Heiser, J. Appl. Phys. **81**, 7900 (1997).
[36]J. G. Simmons, J. Appl. Phys. **34**, 1793 (1963).
[37]M. L. Trouwborst, C. A. Martin, R. H. M. Smit, C. M. Gudon, T. A. Baart, S. J. van der Molen, and J. M. van Ruitenbeek, Nano Lett. **11**, 614 (2011).
[38]I. Bâldea, EPL (Europhys. Lett.) **98**, 17010 (2012).
[39]A. Schenk, *Advanced Physical Models for Silicon Device Simulation*, Computational Microelectronics (Springer, Vienna, 1998), pp. 281–315.
[40]K.-N. Yang, H.-T. Huang, M.-C. Chang, C.-M. Chu, Y.-S. Chen, M.-J. Chen, Y.-M. Lin, M.-C. Yu, S. Jang, M.-C. Yu, and M. Liang, IEEE Trans. Electron Devices **47**, 2161 (2000).
[41]S. Okhonin, P. Fazan, G. Guegan, S. Deleonibus, and F. Martin, Appl. Phys. Lett. **74**, 842 (1999).
[42]N. M. Ravindra and J. Zhao, Smart Mater. Struct. **1**, 197 (1992).
[43]J. Maserjian and N. Zamani, J. Appl. Phys. **53**, 559 (1982).
[44]S. Datta, Nanotechnology **15**, S433 (2004).
[45]S. Illera, J. D. Prades, A. Cirera, and A. Cornet, EPL **98**, 17003 (2012).

[46]S. Illera, J. D. Prades, A. Cirera, and A. Cornet, Sci. World J. **2015**, 426541 (2015).
[47]N. Garcia-Castello, S. Illera, R. Guerra, J. D. Prades, S. Ossicini, and A. Cirera, Phys. Rev. B **88**, 075322 (2013).
[48]W.-C. Lee and C. Hu, IEEE Trans. Electron Devices **48**, 1366 (2001).
[49]D. B. S. Lo and Y. Taur, IBM J. Res. Dev. **43**, 327 (1999).
[50]J. M. Ramírez, Y. Berencén, L. López-Conesa, J. M. Rebled, F. Peiró, and B. Garrido, Appl. Phys. Lett. **103**, 081102 (2013).